


FULL ARTICLE

Reliability assessment on intravascular photoacoustic imaging of lipid: ex vivo animal and human sample validation

Peng Lei^{1,2,5}  | Jiheng Hao³ | Lei Wang^{1,2} | Xue Wen^{1,2} | Kedi Xiong^{1,2} | Pengfei Zhang^{4*} | Liyong Zhang^{3*} | Sihua Yang^{1,2*}

¹MOE Key Laboratory of Laser Life Science and Institute of Laser Life Science, College of Biophotonics, South China Normal University, Guangzhou, China

²Guangdong Provincial Key Laboratory of Laser Life Science, College of Biophotonics, South China Normal University, Guangzhou, China

³Department of Neurosurgery, Liaocheng People's Hospital, Liaocheng, China

⁴Department of Cardiology, Key Laboratory of Cardiovascular Remodeling and Function Research, Qilu Hospital of Shandong University, Jinan, China

⁵Guangdong Institute of Medical Instruments, Guangdong Academy of Sciences, Guangzhou, China

*Correspondence

*Pengfei Zhang, Department of Cardiology, Key Laboratory of Cardiovascular Remodeling and Function Research, Qilu Hospital of Shandong University, Jinan 250012, China.
Email: pengfei-zhang@163.com

*Liyong Zhang, Department of Neurosurgery, Liaocheng People's Hospital, Liaocheng, 252000, China.
Email: 13346256936@163.com

*Sihua Yang, MOE Key Laboratory of Laser Life Science & Institute of Laser Life Science, College of Biophotonics, South China Normal University, Guangzhou 510631, China.
Email: yangsh@scnu.edu.cn

Funding information

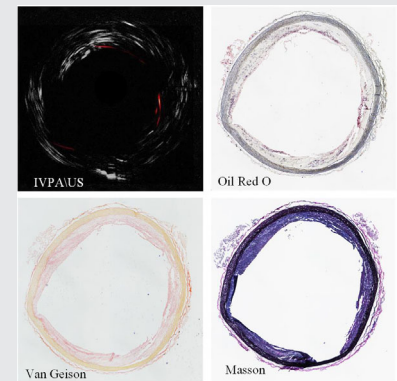
The Science and Technology Program of Guangzhou., Grant/Award Number: 2019050001; National Natural Science Foundation of China, Grant/Award Number: 61822505 61331001 61627827; The Science and Technology Planning Project of Guangdong Province, China, Grant/Award Number: 2015B020233016

Abstract

Although the lipid-detecting IVPA imaging system has been developed in resolution, speed, and catheter size, there is no parameterization study of the reliability on the IVPA imaging for lipid diagnosis. Here, the sensitivity, specificity, and accuracy were calculated to assess the reliability of the IVPA imaging of lipid. Abdominal aortas from six rabbits with atherosclerosis, were subjected to the IVPA imaging and Oil Red O staining, and 75 groups of IVPA as well as corresponding histological images were obtained. Similarly, 125 groups of IVPA and histological results were obtained from five human carotid plaque samples. The sensitivity, specificity, and accuracy, calculated from the statistical data, were 96.8%, 83.3%, 94.6% and 97.3%, 72.7%, 95.2%, respectively. The numerical values of sensitivity, specificity, and accuracy demonstrated the reliability of IVPA imaging on distinguishing the lesions vessel with lipid-rich plaque, which provided the foundation for IVPA translation to clinical application.

KEYWORDS

accuracy, intravascular photoacoustic, lipid, reliability



1 | INTRODUCTION

Cardiovascular diseases (CVDs) are the main cause of mortality and morbidity worldwide. The majority of CVDs events are related to atherosclerosis, a pathology characterized by the formation of plaque in the artery wall.^{1, 2} The evaluation of cardiovascular events must be considered from many aspects, including lipid core size, plaque morphology, fibrous cap thickness, inflammatory activity, macrophage content, intraplaque hemorrhage and other factors. It is well known that the morphology of lipid core is one of key factors that would lead to vulnerable plaque,^{3, 4} and several imaging techniques have been used for lipid detection. Computer tomography angiography (CTA) is easy to find arterial stenosis.⁵ Intravascular ultrasound (IVUS) provides the overall morphology of artery wall for quantification of the plaque burden,⁶ intravascular optical coherence tomography (IVOCT) can detect the thickness of the fiber cap,⁷ and especially, Near-Infrared spectroscopy imaging (NIRS) shows the good sensitivity and specificity for lipid-rich plaque detection.^{8–10} Photoacoustic imaging, an emerging imaging technology, has been proven to specifically image the lipid component as well as the structure information.^{11–16} So far, there is no related study on this topic yet for IVPA imaging validation.

The sensitivity, specificity, and accuracy of IVPA are valuable to be investigated as it is an essential step for clinical translation of IVPA imaging. Specifically, the lipid-specific contrast is generated endogenously from the first overtone absorption of C-H bonds at 1720 nm wavelength (the detail information of absorption spectrum were shown in supporting Figure S1), and the PA signal of lipid is one order of magnitude greater than that of water and connective tissues at this wavelength,^{17, 18} which makes IVPA imaging a promising technology for mapping and assessing the lipid over the entire artery wall.^{19–23}

Although IVPA imaging is constantly developing, the current IVPA researches still focus on improving resolution, imaging depth, and imaging speed.^{24–28} The latest researches showed that the IVPA endoscopic system has the best lateral resolution of 13 μm and has the ultrafine imaging catheter with a diameter of 0.7 mm.^{29, 30} What's more, the imaging speed can achieve 50 frames per second.³¹ All these provide huge support for the IVPA endoscope to translate into clinical application. However, there is no related researches using quantitative parameters to assess the reliability of IVPA imaging of lipid. Sensitivity, specificity, and accuracy are commonly used parameters to evaluate the medical imaging technologies and to quantify how good and reliable a test is. These

parameters have been helped the doctors to judge the reliability of the imaging results.^{32–34} For IVPA imaging of lipid, the sensitivity evaluates how good at detecting the lipid in lesions vessel. Specificity estimates how likely the normal vessel without lipid can be correctly ruled out. Accuracy measures how correct the IVPA imaging identifies and excludes a given condition. Therefore, pre-clinical evaluating the sensitivity, specificity, and accuracy of IVPA imaging of lipid is essential, which can help us understand how the IVPA technology identify the lipid within atherosclerosis plaque. In this article, the sensitivity, specificity, and accuracy assessment on IVPA imaging of lipids were verified on IVPA images and the Oil Red O staining results (gold standard). Ex vivo abdominal aortas in rabbits with atherosclerosis at different stages and the human plaque samples from carotid endarterectomy were conducted for the IVPA imaging and consequently Oil Red O staining, and the comparison results were used to calculate the sensitivity, specificity, and accuracy.

2 | MATERIALS AND METHODS

2.1 | Intravascular Photoacoustic/ultrasound imaging system

Figure 1 was the schematic and photographs of the IVPA/US imaging system. Figure 1A showed the entire IVPA/US working principle diagram: a laser source (NT200 Series Laser, Ekspla, Vilnius, Lithuania) delivered pulsed laser at high pulse repetition rates of 2.5 kHz and laser-pulses duration of approximately 8 ns. The laser wavelength used for the IVPA experiment was 1720 nm. The output laser was spatially attenuated and reshaped, and focused into the input multimode fiber (with core diameter of 50 μm , FG050LGA, Thorlabs, New Jersey) end of the optics and electricity rotary joint (OERJ). The output fiber end of OERJ was connected to the probe. The final output energy of the probe was 20 μJ per pulse and the calculated max energy density was about 200 mJ/cm^2 , which was far below the safety threshold of the ANSI laser safety standard of 1 J/cm^2 at 1720 nm.³⁵ The synchronous output of the laser was used not only to trigger the high-speed data-acquisition card (M-3i.4120, Spectrum, Germany), but also to trigger the pulser and receiver (5073PR, Olympus) after a 10 μs delay by the delay generator (DG535, Stanford Research Systems, Sunnyvale, California). The induced PA/US signals detected by the single-element transducer were amplified by the amplifier with 50 dB gain (LNA-650, RFBAY, Gaithersburg, Maryland) and then digitized with the data-acquisition card at a sampling rate of 250 MHz/s. The raw PA

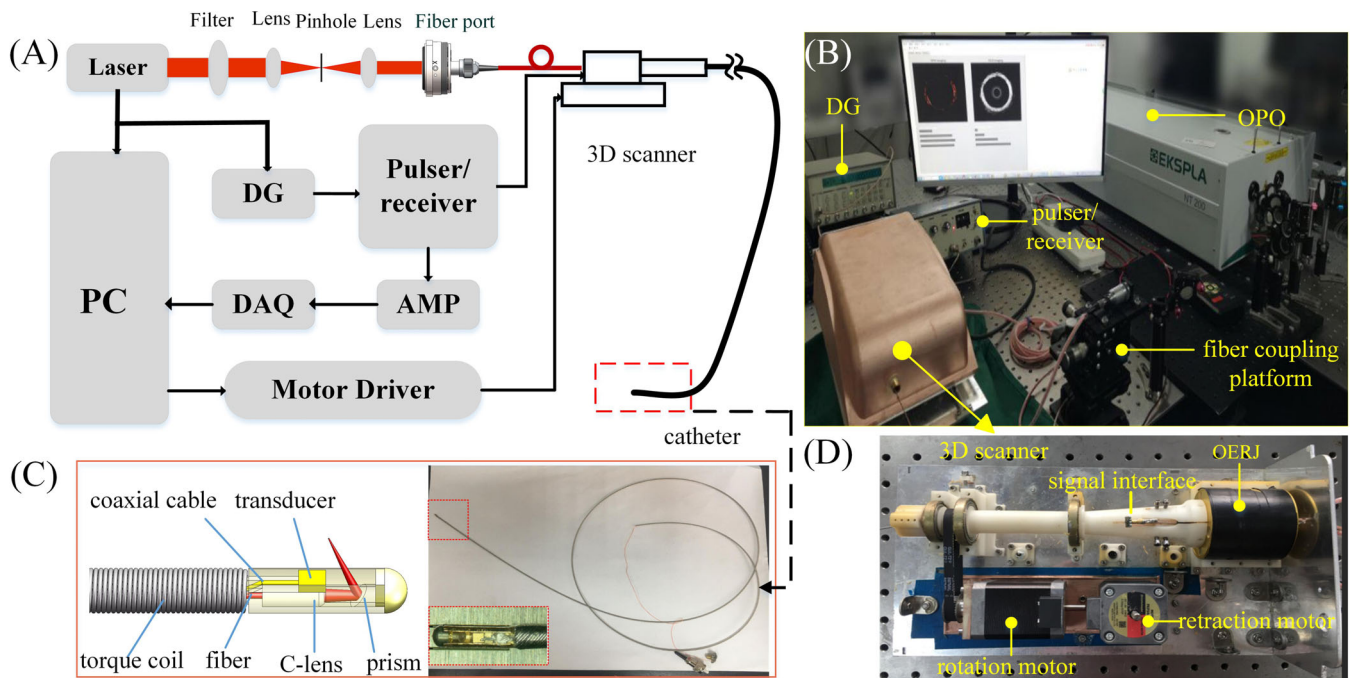


FIGURE 1 Schematic and photographs of the IVPA/US imaging system. (A) Schematic of the IVPA/US dual-mode imaging system. (B) Photograph of the IVPA/US system. (C) The design of the probe and the photograph of the catheter. (D) Photograph of the 3D scanner device. PC: personal computer; AMP: amplifier; DG: delay generator; OPO: optical parametric oscillator; OERJ: optics and electricity rotary joint

signals were filtered using a high pass filter (>5 MHz, 5073PR, Olympus) to remove low-frequency electromagnetic noise. All procedures were controlled by the Labview software, and the data reconstruction were processed by MATLAB. Figure 1B was the photograph of the IVPA/US system. The detailed structural design and photograph of the 3D scanner was shown in Figure 1D. The OERJ was built with an optical-electric rotary (customized, JINPAT, Shenzhen, China) and a rotate and linear platform. The platform consisted of two motors (PKP546N18B-L, Oriental Motor, Japan), which can drive the catheter rotation and retraction in order to get 3D images of the sample. The design of the probe and the photograph of the catheter was shown in Figure 1C. The endoscopic probe integrated 0.5-mm-diameter C-lens (customized, Fuzhou Gongxin Photoelectric Technology Co., Ltd., Fujian, China), 55° prism mirror (customized, Nanyang Jingliang Photoelectric Co., Ltd., Henan, China) and ultrasound transducer with the dimension of 0.5 mm × 0.6 mm × 0.2 mm, and a central frequency of 45 MHz (customized, Blatek, Pennsylvania). The C-lens was used to focus the output laser beam. The fiber, the transducer, the C-lens and the prism were assembled in an ultracompact house, which has a diameter of 1.0 mm. The house was connected into a double-layer torsion coil

(customized, Asahi Intecc, Aichi, Japan). And the catheter, made of the probe and the torque coil, was connected with the OERJ.^{30, 36} In order to precisely assess the sensitivity, specificity and accuracy of intravascular photoacoustic (IVPA) imaging on lipids, the catheter sheath was not used during the ex vivo IVPA experiments. And 500-lines PA signals were averaged five times to acquire a high-quality IVPA B-scan image which corresponding to the imaging speed at one frame per second.

2.2 | Animal preparation

The New Zealand white rabbits were used in the time-lapse experiments, and received 4, 10, 16 weeks of high-fat/high-cholesterol (HFC) diet respectively. The male New Zealand White rabbits with 2 Kg in weight were fed with HFC diet (1% cholesterol) for 1 week before the strain surgery. Then the abdomen aorta endothelium was artificially strained by a 4-Fr balloon catheter through the right femoral artery. After the strain, the rabbits were continued fed with HFC diet. On the fourth week, the tenth week and the sixteenth week after the strain, the rabbits were euthanized with an overdose of pentobarbital (3%, 120 mg/kg). The

abdominal aorta of each rabbit was excised and flushed with PBS (pH 7.4). Six rabbits with atherosclerosis model were cultivated for the research and two rabbits were sacrificed after each feeding cycle. Two segments of the abdominal aorta from the sacrificed rabbit were excised. And each segment has a length of 3.0 mm. The selected segment was promptly examined with IVPA/US imaging. The started position of IVPA/US imaging was marked, and the distance between each cross-section was also fixed. After imaging, the histology procedure was started from the marked position and the same distance samples were abandoned to get another frozen slice, which matched the IVPA/US imaging. The failed histology tissue slices after Oil Red O staining were also abandoned. After all the procedures, 25 matched IVPA/US images and corresponding histology images were obtained from the rabbit samples at each feeding cycle and total 75 groups of data were obtained. The histology analysis was performed by investigators blinded to the IVPA/US results. Finally, the Oil Red O stained lipid area were counted to compare with the IVPA/US imaging results. The animal study was approved by the Animal Study Committee of College of Biophotonics at South China Normal University in Guangdong, China.

2.3 | Statistical analysis

Sensitivity, specificity and accuracy are described in terms of true positive (TP), true negative (TN), false negative (FN), and false positive (FP). In this article, the Oil Red O stained histology results were used as the gold standard to assess the sensitivity, specificity, and accuracy of the IVPA/US imaging system. The relevant definitions are as follows^{37, 38}: the lipid area counted from Oil Red O stained histology results called "H", and the lipid area counted from the IVPA images called "P". If the P was greater than or equal to $0.85H$, but less than or equal to $1.2H$ ($0.85H \leq P \leq 1.2H$), we call the IVPA result TP; if the P was greater than or equal to $.45H$, but less than or equal to $.85H$ ($0.45H \leq P \leq .85H$), we called this TN; if the P was greater than $1.2H$ ($P > 1.2H$), we called this FP; if the P was less than $.45H$ ($P < .45H$), we called this FN. After those circumstances were counted, the sensitivity, specificity and accuracy can be calculated as follows: Sensitivity = $TP/(TP + FN)$ = (Number of TP assessment)/(Number of all positive assessment); Specificity = $TN/(TN + FP)$ = (Number of TN assessment)/(Number of all negative to assess the assessment); Accuracy = $(TP + TN)/(TP + TN + FP + FN)$ = (Number of correct assessments)/Number of all assessments). Data

were presented as mean \pm SD. The correlation between IVPA and Oil Red O stained histology results were tested with linear correlation using Origin (OriginLab, Northampton). The Bland–Altman tests were performed to determine the agreement between them with MedCalc (MedCalc software).

3 | RESULTS

3.1 | Resolution evaluation of the IVPA/US system

To verify the lateral and axial resolution of the IVPA/US imaging system, IVPA/US imaging of a carbon fiber with a diameter of 10 μm was performed. The carbon fiber was immersed in a hollow gelatin phantom as a target and the depth-resolved PA B-scan images with 500 A-lines were acquired. The distance between the probe tip and the carbon fiber was 2.5 mm. Figure 2A, E were IVPA and IVUS B-scan images obtained by the system, respectively. Figure 2B was an enlarged view of the dotted-line box in Figure 2A. Figure 2C,D were the lateral and the axial resolutions of the IVPA system, respectively. The lateral and the axial pixel width were utilized as the line spread functions (LSPs) to evaluate the lateral and the axial resolution, and the lateral resolution of IVPA system was 109 μm , while the axial resolution was 49 μm . Figure 2F was an enlarged view of the dotted line box in Figure 2E. Figure 2G,H were the lateral and the axial resolution of the IVUS system, respectively. The lateral resolution of IVUS system was 148 μm , while the axial resolution was 38 μm . The calculated lateral and axial resolution of the IVPA system were equivalent to the clinical IVUS resolution,⁶ which indicated that the IVPA imaging results of lipid was convincing and the results can be used to assess the sensitivity, specificity and accuracy.

To further verify the resolution variety of the IVPA/US imaging system, the IVPA imaging of tungsten wires with a diameter of 10 μm at different depths were performed. The photographs of the spot size from the probe tip at different distances were captured by a beam analyzer. Figure 3A was the pictures of spot size at different distance, and Figure 3B was the relevant spot diameters obtained by statistically analyzing the results of Figure 3A. Figure 3C was the schematic diagram of the distribution of 10 μm diameter tungsten wires at different depths in agar, and Figure 3D was obtained corresponding IVPA image of the tungsten. From the B-scan IVPA image, it can be seen that the distribution of tungsten wires at different depths that can be projected by IVPA imaging, and the result was

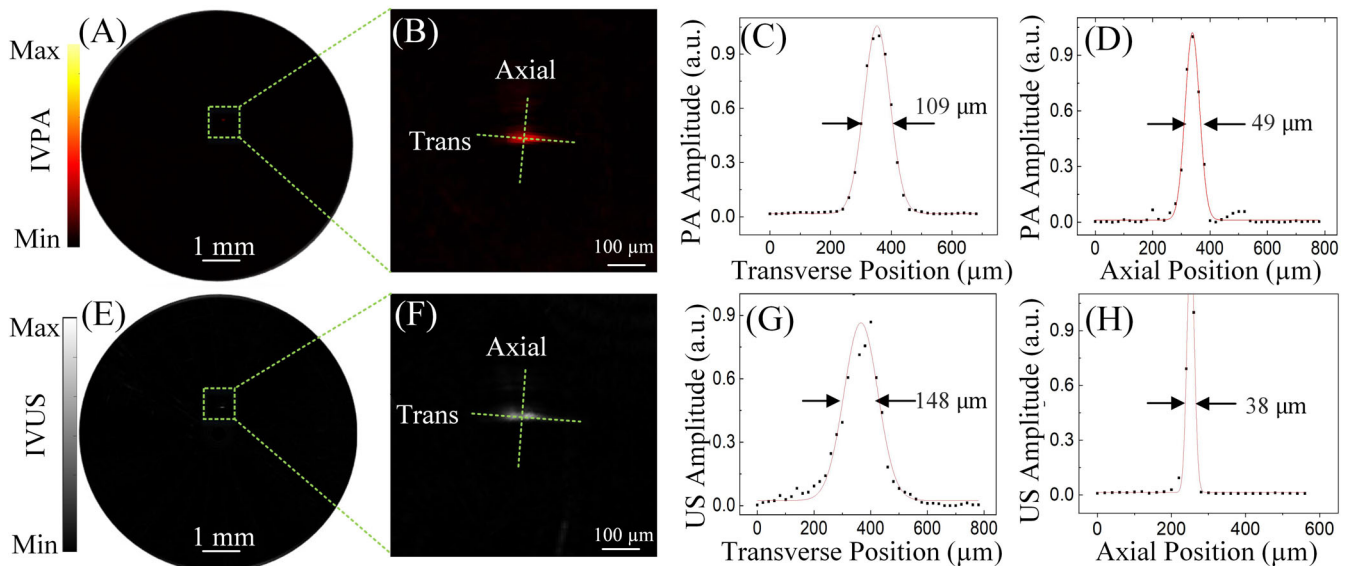


FIGURE 2 The lateral and the axial resolution of IVPA/US imaging system. (A) IVPA B-scan image of the carbon fiber (10 μm in diameter). (B) Enlarged view of dotted-line box in (A). (C) The lateral resolution of IVPA imaging system. (D) The axial resolution of IVPA imaging system. (E) IVUS B-scan image of the carbon fiber. (F) Enlarged view of the dotted-line box in (E). (G) The lateral resolution of IVUS system. (H) The axial resolution of IVUS system. IVPA, intravascular photoacoustic; IVUS, intravascular ultrasound

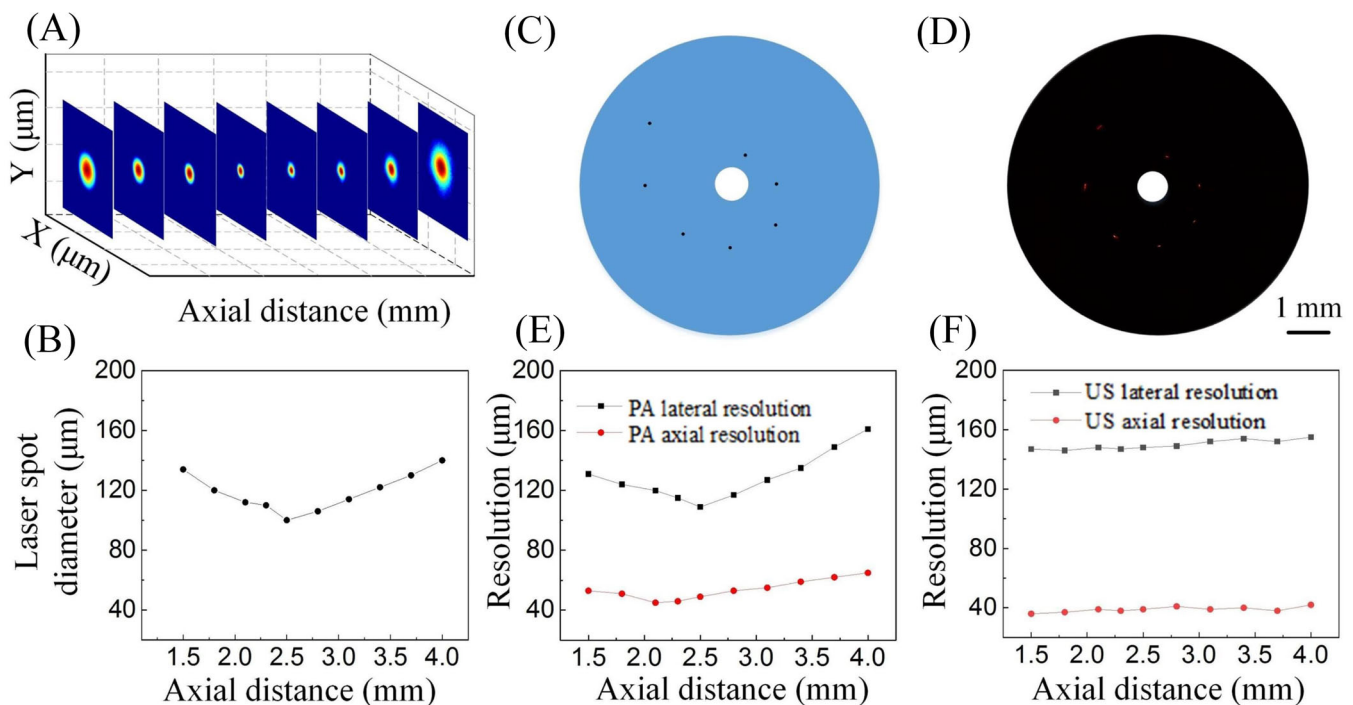


FIGURE 3 The stability of the IVPA/US System. (A) The photographs of the light spot of the probe along the axial distance. (B) The diameters of the light spot along the axial distance. (C) The schematic of the sample distribution. (D) The IVPA B-scan image of the tungsten wires. (E) The resolution of IVPA system along the axial distance. (F) The resolution of IVUS system along the axial distance

almost same as the actual distribution. Figure 3E was the curve of IVPA lateral resolution and axial resolution along the axial distance. The best lateral resolution

of IVPA imaging was about at 2.5 mm, which also corresponded to the laser focal point position. The curve of IVUS lateral and axial resolution along the axial

distance was also shown in Figure 3F. When the IVPA/US imaging catheter intervenes into the blood vessel, the catheter probe may not necessarily in the center of

the lumen. The above results indicated that the IVPA imaging still have good performance even the probe was eccentric in the vessel lumen.

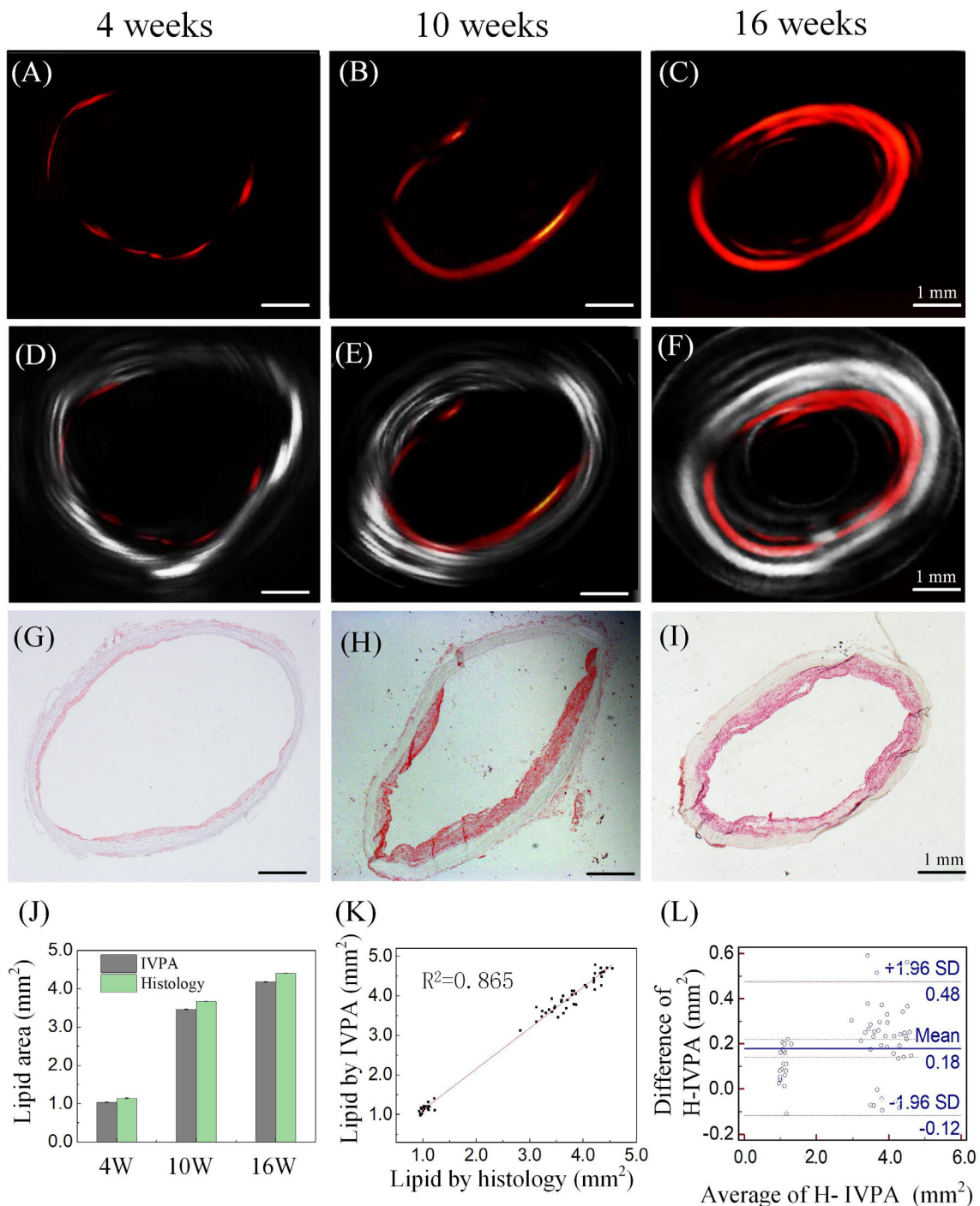


FIGURE 4 The IVPA/US images of the rabbits' abdominal aortas at the fourth, the tenth and the sixteenth week. (A-C) The IVPA images of the rabbit abdominal aorta at the fourth week, tenth week and sixteenth week after surgery, respectively. (D-F) The merged IVPA and IVUS images of the rabbits' abdominal aorta at the fourth week, tenth week and sixteenth week after surgery, respectively. (G-I) The corresponding Oil Red O stained histology images. (J) The average of lipid area counted in IVPA imaging and histological staining. (K) The correlation between lipid area by histology and IVPA imaging. (L) Bland-Altman tests of IVPA and histology. IVPA: intravascular photoacoustic, H: histology, 4 W: 4 weeks, 10 W: 10 weeks, 16 W: 16 weeks

3.2 | IVPA/US imaging experiments of rabbit abdominal aortas

In order to calculate the sensitivity, specificity and accuracy of the lipid of intravascular photoacoustic imaging, the abdominal aortas from rabbits with atherosclerotic model at different stages were used for the IVPA/US imaging and Oil Red O staining.

The IVPA images, IVPA/US merged images and corresponding frozen section Oil Red O stained results of the rabbits' abdominal aortas were shown in Figure 4. Each stage of the rabbit's abdominal aorta was selected, and one representative cross-section images was displayed in the Figure 4. It can be seen from the Oil Red O stained results that after HFC diet feed, there was a small amount of lipid accumulation in the abdominal aorta at the fourth week, and the IVPA image in Figure 4A also showed the little lipid distribution. Meanwhile the merged IVPA/US image in Figure 4D confirmed that the lipid was from inner wall of the vessel. After 10 weeks HFC diet feed, the other abdominal aortas of rabbits were also subjected to IVPA/US imaging. As shown in Figure 4B, the IVPA image showed that the lipid accumulation in aorta increased with the longtime of HFC diet feeding. The Oil Red O stained slice image in Figure 4H also verified the increased lipid accumulation and matched the IVPA image well. Figure 4B,E,H showed the IVPA, IVPA/US merged image, and stained images of the

aorta at the tenth week. Finally, the abdominal aortas from rabbit with 16 weeks HFC diet fed were subjected to the IVPA/US imaging. Similar to the previous imaging results, the IVPA image in Figure 4C showed a more obvious increase in lipid content, and the lipid in IVPA imaging was close to the result of staining (Figure 4I).

Figure 4J illustrated the average of lipid area counted in IVPA imaging and histological staining. Figure 4K showed the correlation between all the IVPA imaging results and the Oil Red O staining results. It can be seen that the correlation coefficient was about 0.865. Both the results of two methods were also analyzed with Bland-Altman analysis (Figure 4L). It can be seen that the scatter points almost distributed with the consistency limit of 95% from Figure 4L, confirming the consistency between the IVPA imaging and Oil Red O staining. The IVPA/US imaging of three groups of rabbits' abdominal aortas at different stages demonstrated that the results of IVPA imaging of lipid have a high correlation with Oil Red O staining results.

To further demonstrate that the IVPA imaging of lipids had high correlation with the Oil Red O stained results, the zoom-in IVPA and histology images were compared in the radial direction in Figure 5. Two representative areas of lipid in the IVPA image (I, II) and the histology image (I', II') were picked to show the detail radial distribution of the lipid. Figure 5A was the IVPA image, two representative areas in white dotted

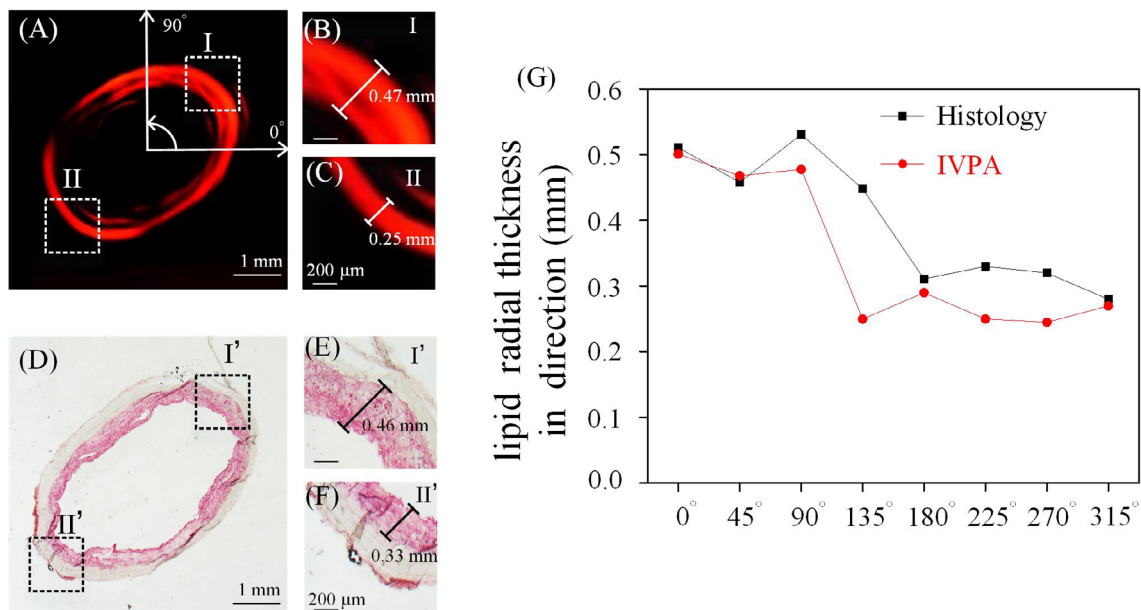


FIGURE 5 The lipid thickness distribution in radial direction in IVPA and histology images. (A) The image of lipid distribution reconstructed by IVPA imaging. (B), (C) The zoom-in view of the white dotted box in (A). (D) The Oil Red O stained frozen section result of lipid. (E), (F) The zoom-in view of the white dotted box in (D). (G) The curve of lipid thickness variety from 0° to 360°

box were chosen to verify the thickness of the lipid in the radial direction. Figure 5B,C were the zoom-in view of the white dotted box, and the lipid thickness were 0.47 mm and 0.25 mm, respectively. Similarly, two corresponding representative areas (black dotted box) in the histology image were also picked, and the zoom-in view of the artery were shown in Figure 5E,F. The thickness of the lipid in area I' and II' were 0.46 mm and 0.33 mm, respectively. The thickness of lipid measured from the IVPA and histology results were very close. Further, the lipid thickness from 0° to 360° were also measured and shown in Figure 5G. From the two curves, it can be seen that the distribution of lipid thickness was basically consistent in IVPA and histological staining results.

The lipid area by IVPA imaging and the Oil Red O staining were counted by IPP software, and the numbers of TP, TN, FN and FP were shown in Table 1. And the P Value refers to the comparison of lipid area by IVPA and Oil Red O staining in each different stage. From Table 1, the sensitivity, specificity, and accuracy can be calculated, and the results were 96.8%, 83.3%, and 94.6%.

To better understand plaque features in relationship with the morphology, the IVPA\US imaging, the Oil Red O stain, Masson stain, Verhoeff-van Gieson stain of rabbit aorta (the rabbit has been fed with high fat diet for more than 6 months) were also conducted to analysis the elastin and collagen. The results were shown as follows: From Figure 6A,D it can be seen that the lipid area reconstructed by IVPA imaging were consistency with the Oil Red O stained result. The Verhoeff-van Gieson stained results in Figure 6E showed the fibrosis of the plaque. The stained red area depicted the collagen fibers of the plaque and the stained yellow area showed that the muscle fibers of vessel wall. The red area in the Verhoeff-van Gieson stained image indicated that the plaque has developed into fibrous plaque. And this result was also confirmed by the Masson stain. The IVPA result, the Verhoeff-van Gieson stain results and the Masson stain results (Figure 6F) depicted that even if the plaque developed into hyperfibrosis, the IVPA imaging would not misdiagnosis the collagen fibers as lipid.

3.3 | Ex vivo IVPA imaging experiments of human carotid plaque

To further investigate the IVPA imaging of lipids, the human carotid plaque samples were used for assessing the sensitivity, specificity, and accuracy. Ethical approval for this study was obtained from the Liaocheng People's hospital. Human carotid plaques, harvested from the carotid endarterectomy, were obtained from five patients with stenosis. The human sample were obtained from the carotid plaques not the arterial segment. Human sample 1 were obtained by the Eversion carotid endarterectomy, and human sample 2 to 5 were obtained by the Standard carotid endarterectomy. The detailed surgical procedure of the Standard and Eversion carotid endarterectomy were shown in the supporting material. Before the carotid endarterectomy, these patients underwent CTA to locate the lesions in the carotid. After the carotid endarterectomy, the carotid plaques were stored in formalin before imaging, and were fixed with gelatin when the IVPA/US imaging conducted.³⁹ The same procedures were conducted to get matched IVPA images and the Oil Red O staining images as mentioned before. After all the procedures, 125 matched IVPA/US images and frozen section Oil Red O stained images were acquired. The experimental results were shown in Figure 6. Each row in Figure 7 shows the CTA angiographic results, photographs of the sample, IVPA images, merged IVPA/US images and the Oil Red O stained slice images of the human carotid plaques. From the IVPA images and staining results, it can be seen that the lipid area is basically consistent.

The lipid area by IVPA imaging and the Oil Red O stained were also counted by IPP software, and the numbers of TP, TN, FN and FP were shown in Table 2. From Table 2, the sensitivity, specificity and accuracy can be calculated, and the results were 97.3%, 72.7%, and 95.2%.

3.4 | Statistical results

The sensitivity, specificity, and accuracy of the rabbits' aorta plaque and five human carotid plaques,

TABLE 1 Comparison of IVPA results with histological staining (gold standard) in rabbits with atherosclerosis

	True positive	False positive	True negative	False negative	P value
4 weeks	20	1	4	0	.0037
10 weeks	21	0	3	1	.0005
16 weeks	20	1	3	1	.0066
Total (n = 75)	61	2	10	2	

Note: P value refers to the comparison of lipid area by IVPA and Oil Red O staining in each rabbit at different stage.

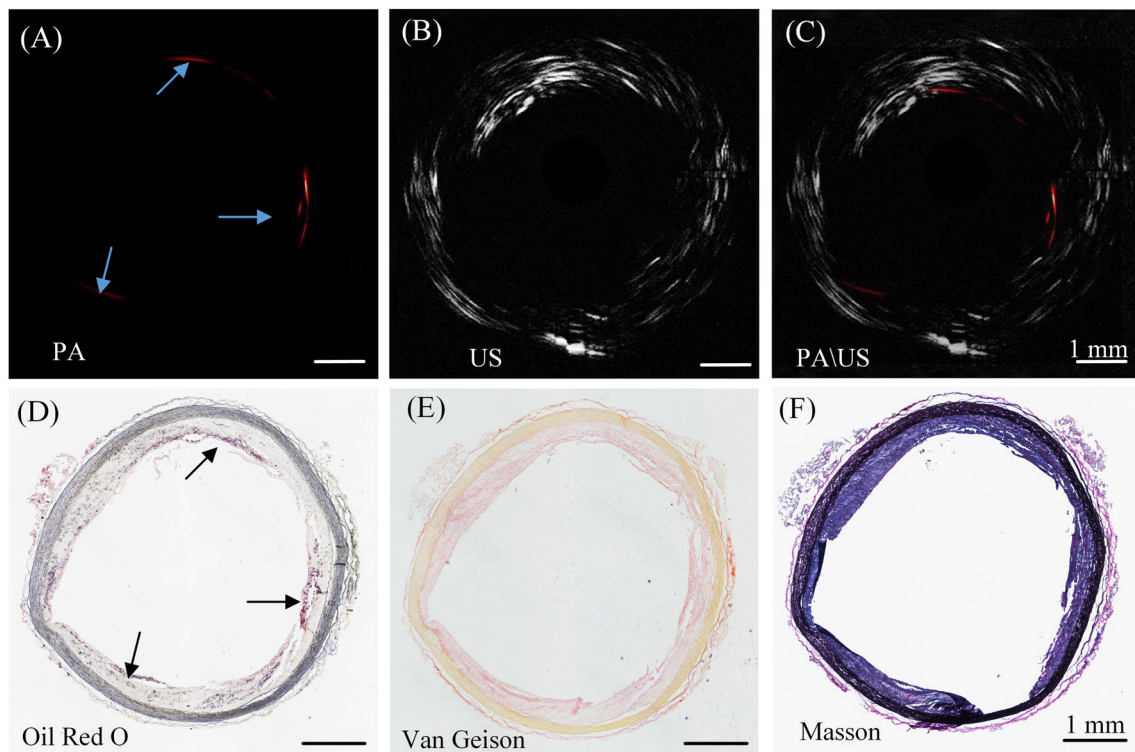


FIGURE 6 The IVPA\US images and the stained images of rabbit abdominal aorta. (A) The IVPA image of the rabbit abdominal aorta. (B) The US image of the rabbit abdominal aorta. (C) The merged IVPA\US image of the rabbit abdominal aorta. (D) The Oil Red O stained image of the rabbit abdominal aorta. (E) The Van Gieson stained image of the rabbit abdominal aorta. (F) The Masson stained image of the rabbit abdominal aorta

calculated from the 75 and 125 groups of data, were shown in Table 3. The sensitivity, specificity, and accuracy of the IVPA imaging in rabbit abdominal aorta and human plaque from carotid endarterectomy were 96.8%, 83.3%, 94.6% and 97.3%, 72.7%, 95.2%, respectively. The components of human carotid plaque may include lipids, fibrosis, calcification and intraplaque hemorrhage et al. The fibrosis and calcification would influence the penetration depth of the laser, which would influence the statistical results from the IVPA images and in turn, the sensitivity, specificity and accuracy would change. However, the specificity of both were more than 72%, which was still acceptable. From Table 3, it can be seen that the sensitivity of the IVPA system for lipid diagnosing on rabbit aortas and the human plaques surpassed 96%, which indicated the IVPA imaging system has 96% probability for diagnosing the lipid in the atherosclerosis plaques, and this was an excellent performance. And the accuracy of the IVPA imaging system exceeded 93%. The high value of accuracy illustrated that the IVPA imaging has a correct lipid diagnosis rate no less than 93%. In general, the numerical values of sensitivity, specificity, and accuracy verified the reliability of the IVPA imaging for lipid diagnosis.

4 | DISCUSSION AND CONCLUSION

Reliability assessment on the intravascular photoacoustic imaging of lipid is one of the most important pre-clinical procedures to evaluate the IVPA system. In this regard, the rabbits with atherosclerosis and the human plaques from carotid endarterectomy were conducted to the IVPA imaging and compared to the Oil Red O staining result (gold standard). The ex vivo experiment results showed that the sensitivity, specificity and accuracy of IVPA imaging for lipid detecting were almost equivalent to histology. But the present study does have some limitations. For example, the catheter performance of the IVPA system may differ from catheter to catheter, and that would lead to the difference between the IVPA images on rabbit and human sample. The electronic noise and other absorbers may cause the artifacts in the IVPA images and that would lead to the low specificity. And for the in vivo experiment, the heartbeat, the respiratory pulsation and the sheath of the catheter, which may also lead the artifacts in the IVPA imaging,^{25, 40} would increase the numbers of FP, and that in turn would influence the specificity. In future studies, it is also necessary to increase the number of samples and add the normal

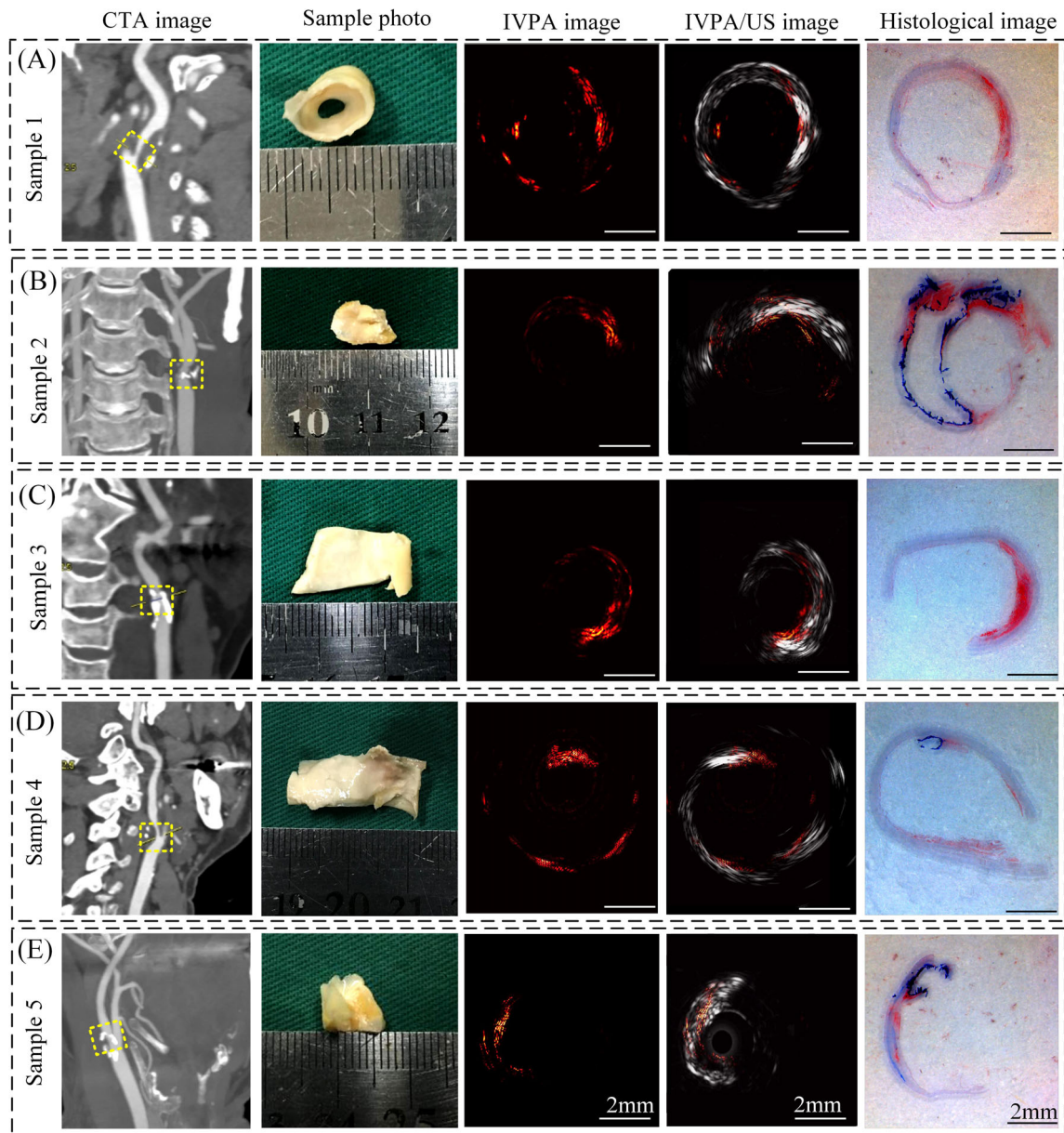


FIGURE 7 The CTA, photographs, IVPA images, merged IVPA/US images and histology stained results of the 5 human carotid plaques. (A) The CTA image, photograph of sample, IVPA image, merged IVPA/US image and Oil Red O stained result of the human carotid plaque from a 67 years old man. (B) The CTA image, photograph, IVPA image, merged IVPA/US image and Oil Red O stained result of the human carotid plaque from a 63 years old man. (C) The CTA image, photograph, IVPA image, merged IVPA/US image and Oil Red O stained result of the human carotid plaque from a 71 years old woman. (D) The CTA image, photograph, IVPA image, merged IVPA/US image and Oil Red O stained result of the human carotid plaque from a 66 years old man. (E) The CTA image, photograph, IVPA image, merged IVPA/US image and Oil Red O stained result of the human carotid plaque from a 72 years old woman

vessel samples as TN to further calculate the sensitivity, specificity, and accuracy. Another limitation of this study was that the sensitivity, specificity and accuracy depends on system and the criteria used to define the abnormality. The result would vary when using other systems and criteria.

In summary, for the first time, the sensitivity, specificity, and accuracy were calculated from the rabbits' aortas

and human plaques from carotid endarterectomy to assess the reliability of IVPA for lipid diagnosis. The IVPA imaging system can achieve the best photoacoustic lateral resolution and axial resolution of $109\ \mu\text{m}$ and $49\ \mu\text{m}$, respectively. At the same time, The IVPA imaging system has the good resolution within a certain range of depth changes. The IVPA imaging results of the abdominal aortic of rabbits at different periods and human

TABLE 2 Comparison of IVPA results with histological staining (gold standard) in human plaques

	True positive	False positive	True negative	False negative	P value
Sample 1	22	1	2	0	.1911
Sample 2	22	1	1	1	.0156
Sample 3	23	0	1	1	.0206
Sample 4	22	1	2	0	.054
Sample 5	22	0	2	1	.0311
Total (n = 125)	111	3	8	3	

Note: P value refers to the comparison of lipid area by IVPA and Oil Red O staining in each human plaque.

TABLE 3 The statistical results of PA imaging of different human carotid plaques

Sample type	Sensitivity	Specificity	Accuracy
Rabbit aorta sample	96.8%	83.3%	94.6%
Human carotid plaque	97.3%	72.7%	95.2%

carotid plaques have high consistency with the Oil Red O stained results. The sensitivity, specificity, and accuracy of the IVPA imaging in rabbit abdominal aorta and human plaque from carotid endarterectomy were 96.8%, 83.3%, 94.6% and 97.3%, 72.7%, 95.2%, respectively. The numerical value of sensitivity indicated that the IVPA imaging has great probability of diagnosing lipid and the specificity illustrated that the IVPA imaging owns the good ability for not misdiagnose the normal vessel without plaque. The accuracy also verified the reliability of IVPA imaging for lipid diagnosis. The numerical values of sensitivity, specificity and accuracy verified the reliability of IVPA imaging for lipid diagnosis, which provided an important foundation for the IVPA translation to clinical application.

ACKNOWLEDGMENT

This research was supported by the National Natural Science Foundation of China (61822505, 61331001, 61627827); The Science and Technology Planning Project of Guangdong Province, China (2015B020233016); The Science and Technology Program of Guangzhou (2019050001).

CONFLICTS OF INTEREST

The authors declare no potential conflict of interest.

DATA AVAILABILITY STATEMENT

The data that support the findings of this study are available from the corresponding author upon reasonable request.

ORCID

Peng Lei  <https://orcid.org/0000-0002-1969-0035>

REFERENCES

- [1] D. S. Celermajer, C. K. Chow, E. Marijon, N. M. Anstey, K. S. Woo, *J. Am. Coll. Cardiol.* **2012**, 60(14), 1207.
- [2] World Health Organization. Cardiovascular diseases (CVDs). **2018**. <http://www.who.int/mediacentre/factsheets/fs317/en/>
- [3] F. D. Kolodgie, R. Virmani, A. P. Burke, *Heart* **2004**, 90(12), 1385.
- [4] R. Virmani, F. D. Kolodgie, A. P. Burke, A. Farb, S. M. Schwartz, *Arterioscler. Thromb. Vasc. Biol.* **2000**, 20(5), 1262.
- [5] S. Debernardi, L. Martincich, D. Lazzaro, S. Comelli, A. M. Raso, D. Regge, *Radiol. Med.* **2004**, 108(1–2), 116.
- [6] T. Kubo, A. Maehara, S. Gary, H. Mintz, K. T. Doi, S.-Y. Choi, O. Kato, K. Nasu, A. Koenig, M. Pieper, J. H. Rogers, W. Wijns, D. Bose, M. P. Margolis, J. W. Moses, G. W. Stone, M. B. Leon, *J. Am. Coll. Cardiol.* **2010**, 55(15), 1590.
- [7] H. Jia, F. Abtahian, A. D. Aguirre, S. Lee, S. Chia, H. Lowe, K. Kato, T. Yonetsu, R. Vergallo, S. Hu, J. Tian, H. Lee, S. J. Park, O. C. Yang-Soo Jang, K. Raffel, S. Mizuno, T. Uemura, T. K. Iton, S.-Y. Choi, H. L. Dauerman, A. Prasad, C. Toma, I. McNulty, S. S. Zhang, R. Virmani, I.-K. Jang, *J. Am. Coll. Cardiol.* **2013**, 62(19), 1748.
- [8] C. M. Gardner, H. Tan, E. L. Hull, J. B. Lisauskas, S. T. Sum, M. M. Thomas, C. Jiang, P. M. Sean, J. D. Caplan, A. P. Burke, R. Virmani, J. Goldstein, J. E. Muller, *JACC Cardiovasc. Imaging* **2008**, 1, 638.
- [9] S. Brugaletta, M. Sabaté, *Circ. J.* **2014**, 78, 1531.
- [10] D. Erlinge, *J. Intern. Med.* **2015**, 278, 110.
- [11] L. V. Wang, S. Hu, *Science* **2012**, 335(6075), 1458.
- [12] H. Guo, Q. Chen, W. Qi, X. Chen, L. Xi, *J. Biophotonics* **2018**, 11(9), e201800067.
- [13] B. Dong, S. Chen, Z. Zhang, C. Sun, H. F. Zhang, *Opt. Lett.* **2014**, 39(15), 4372.
- [14] P. Fei, J. Nie, J. Lee, Y. Ding, S. Li, H. Zhang, M. Hagiwara, T. Yu, T. Segura, C.-m. Ho, D. Zhu, T. K. Hsiai, *Adv. Photonics* **2019**, 1(1), 016002.
- [15] A. Hussain, E. Hondebrink, J. Staley, W. Steenbergen, *Optica* **2018**, 5(12), 1579.

- [16] Y. Li, R. Lin, C. Liu, J. Chen, H. Liu, R. Zheng, X. Gong, L. Song, *J. Biophotonics* **2018**, *11*(10), e201800034.
- [17] H. Wang, N. Chai, P. Wang, W. Dou, D. Umulis, L. V. Wang, M. Sturek, R. Lucht, J. Cheng, *Phys. Rev. Lett.* **2011**, *106*(23), 238106.
- [18] J. Hui, R. Li, E. H. Philips, C. J. Goergen, M. Sturek, J. Cheng, *Photoacoustics* **2016**, *4*(1), 11.
- [19] S. Hu, P. Yan, K. Maslov, J. M. Lee, L. V. Wang, *Opt. Lett.* **2009**, *34*(24), 3899.
- [20] X. Li, J. C. Yin, C. H. Hu, Q. F. Zhou, K. K. Shung, Z. P. Chen, *Appl. Phys. Lett.* **2010**, *97*(13), 133702.
- [21] J. M. Yang, K. Maslov, H. C. Yang, Q. Zhou, K. K. Shung, L. V. Wang, *Opt. Lett.* **2009**, *34*(10), 1591.
- [22] P. D. Kumavor, U. Alqasemi, B. Tavakoli, H. Li, Y. Yang, X. Song, E. Warych, Q. Zhu, *J. Biophotonics* **2013**, *6*(6–7), 475.
- [23] B. Bungart, Y. Cao, T. Yang-Tran, S. Gorsky, L. Lan, D. Roblyer, M. Koch, L. Cheng, T. Masterson, J. X. Cheng, *Biomed. Opt. Express* **2019**, *10*(3), 1405.
- [24] J. Zhang, S. H. Yang, X. R. Ji, Q. Zhou, D. Xing, *J. Am. Coll. Cardiol.* **2014**, *64*(4), 385.
- [25] B. Wang, J. L. Su, J. Amirian, S. H. Litovsky, R. Smalling, S. Emelianov, *Opt. Express* **2010**, *18*(5), 4889.
- [26] Y. C. Cao, A. Kole, J. Hui, Y. Zhang, J. Y. Mai, M. Alloosh, M. Sturek, J. X. Cheng, *Sci. Rep.* **2018**, *8*(1), 2400.
- [27] X. S. Bai, X. J. Gong, W. Hua, R. Lin, J. Zheng, C. Liu, C. Zeng, X. Zou, H. Zheng, L. Song, *PLOS One* **2014**, *9*(3), 92463.
- [28] S. Iskander-Rizk, M. Wu, G. Springgeling, H. Beusekom, F. Mastik, M. Hekkert, R. Beurskens, A. Hoogendoorn, E. Hartman, A. van der Steen, J. J. Wentzel, G. Van Soest, *EuroIntervention* **2019**, *15*(10), 452.
- [29] X. R. Ji, K. D. Xiong, S. H. Yang, D. Xing, *Opt. Express* **2015**, *23*, 9130.
- [30] P. Lei, X. Wen, L. Wang, P. Zhang, S. Yang, *Opt. Lett.* **2019**, *44* (22), 5406.
- [31] Y. Li, Z. Zhu, J. C. Jing, J. J. Chen, A. E. Heridari, Y. He, J. Zhu, T. Ma, M. Yu, Q. Zhou, Z. Chen, *IEEE J. Sel. Top. Quantum Electron.* **2019**, *25*(1), 7102005.
- [32] A. G. Glaros, B. K. Rex, *J. Clin. Psychol.* **1988**, *44*(6), 1013.
- [33] W. Zhu, N. Zeng, N. Wang, Paper presented at the NESUG (North East SAS Users Group), *Health Care and Life Sciences Conference*, Maryland, Baltimore **2010**.
- [34] W. A. Berg, L. Gutierrez, M. S. NessAiver, W. Carter, M. Bhargavan, R. S. Lewis, M. B. Loffe, *Radiology* **2004**, *233*(3), 830.
- [35] Laser Institute of America, *American National Standard for Safe Use of Lasers ANSI Z136.1–2014*, American National Standards Institute, Inc. **2014**.
- [36] L. Wang, P. Lei, X. Wen, P. Zhang, S. Yang, *Opt. Express* **2019**, *27*(9), 12832.
- [37] B. Nyfeler, W. Pichler, *Clin. Exp. Allergy* **1997**, *27*(2), 175.
- [38] R. T. Chang, O. J. Knight, W. J. Feuer, D. L. Budenz, *Ophthalmology* **2009**, *116*(12), 2294.
- [39] M. Xu, P. Lei, J. Feng, F. Liu, S. Yang, P. Zhang, *Chin. Opt. Lett.* **2018**, *16*(3), 031702.
- [40] A. Karpiouk, B. Wang, J. A. Mirian, R. Smalling, S. Emelianov, *J. Biomed. Opt.* **2012**, *17*(9), 096008.

SUPPORTING INFORMATION

Additional supporting information may be found online in the Supporting Information section at the end of this article.

How to cite this article: Lei P, Hao J, Wang L, et al. Reliability assessment on intravascular photoacoustic imaging of lipid: ex vivo animal and human sample validation. *J. Biophotonics*. 2020; e202000162. <https://doi.org/10.1002/jbio.202000162>